CELL BIOLOGY

Clathrin-coated structures support 3D directed migration through local force transmission

Enzo Bresteau*, Nadia Elkhatib, Francesco Baschieri, Karen Bellec†, Mélanie Guérin, Guillaume Montagnac*

Migrating cells navigate in complex environments through sensing and interpreting biochemical and/or mechanical cues. Here, we report that recently identified tubular clathrin/AP-2 lattices (TCALs), a subset of clathrin-coated structures (CCSs) that pinch collagen fibers, mechanically control directed migration along fibers decorated with ligands of CCS cargoes in three-dimensional (3D) environments. We observed that epidermal growth factor or low-density lipoprotein bound to collagen fibers leads to increased local nucleation and accumulation of TCALs. By using engineered, mixed collagen networks, we demonstrate that this mechanism selectively increases local forces applied on ligand-decorated fibers. We show that these effects depend on the ligand's receptors but do not rely on their ability to trigger signaling events. We propose that the preferential accumulation of TCALs along ligand-decorated fibers steers migration in 3D environments. We conclude that ligand-regulated, local TCAL accumulation results in asymmetric force distribution that orients cell migration in 3D environments.

INTRODUCTION

Clathrin-mediated endocytosis is a fundamental process that regulates the uptake of a wide diversity of cell surface receptors and their ligands (*1*). By doing so, clathrin-coated structures (CCSs) impinge on many cellular functions including cytokinesis (*2*), cell migration, and cell invasion (*3*). We recently demonstrated that in three-dimensional (3D) environments composed of collagen fibers, β_1-integrin–enriched CCSs wrap around and pinch fibers, thus providing many anchoring points that facilitate cell migration (*4*). These collagen fiber–pinching CCSs, also called tubular clathrin/AP-2 lattices (TCALs), are frustrated in nature as they try and fail to internalize fibers that are longer than the cell itself (*5*). However, although their lifetime is longer as compared to non–fiber-engaged CCSs, it is still limited in time, suggesting that they may be able to bud and to produce endocytic vesicles after an initial period of frustration on fibers. Collagen fibers are sticky structures to which many proteins can bind or adsorb (*6*). Besides other extracellular matrix (ECM) components, some cytokines and growth factors can also directly or indirectly bind to collagen fibers (*7*). For example, the epidermal growth factor (EGF) was reported to bind to collagen fibers with an estimated affinity of 1.706 μM (*8*). The EGF receptor (EGFR) is mostly internalized through CCSs, and this has been suggested to play a role in chemotaxis toward EGF gradients (*9*, *10*). Low-density lipoprotein (LDL), the ligand of another major CCS cargo, was also reported to bind to collagen fibers (*11*). We set out here to investigate the relationship between TCALs and two major CCSs cargos, and their role in orienting cell migration in 3D environments.

RESULTS AND DISCUSSION

Production and characterization of ligand-decorated collagen fibers

We observed that incubating Alexa488-labeled EGF with a prepolymerized fibrillar collagen gel leads to an accumulation of EGF along fibers (fig. S1A), thus confirming previous findings (*8*). Similar results were obtained when using decellularized liver matrix, suggesting that EGF can also bind physiological collagen fibers (fig. S1B). Because a collagen gel is difficult to handle to address specific questions, we set up a protocol to produce and manipulate chopped collagen fibers decorated with EGF (Fig. 1A). Our protocol produces collagen fibers of quite homogeneous length (15.3 ± 2.3 μm) that can be spotted on glass or incorporated into a 3D network (Fig. 1, B and C). These fibers could be homogeneously decorated with Alexa488-EGF (Fig. 1B) and Dil-LDL (fig. S1C). Long-term imaging (24 hours) of Alexa488-EGF–decorated fibers embedded in a 3D network showed that EGF remains stably associated with fibers (fig. S1D). In addition, fluorescence recovery after photobleaching (FRAP) assays showed that the fluorescence associated with Alexa488-EGF did not recover when engineered fibers were spotted on 2D surfaces or incorporated into 3D networks (fig. S1, E and F). When free Alexa488-EGF was added in the medium before the FRAP experiments, a mobile fraction of approximately 50% was detected (fig. S1, E and F). The immobile fraction observed in this latter experiment most likely corresponds to the EGF fraction that is stably associated with collagen fibers recovered at the end of our production protocol.

We observed that fiber-associated EGF was able to activate the mitogen-activated protein kinase (MAPK) Erk as efficiently as free EGF alone when MDA-MB-231 cells and fibers were incubated together in suspension (fig. S2, A and B). Notably, Erk signaling was more sustained over time when EGF was bound to collagen fibers, suggesting that the frustrated endocytosis process occurring on collagen fibers delays EGFR signaling shutdown. In addition, MDA-MB-231 cells were able to internalize fiber-bound EGF as evidenced by the transfer of EGF-associated fluorescence from the fibers to internal compartments (fig. S2, C and D). We next took advantage of our protocol to generate composite 2D substrates by sequentially spotting EGF-decorated and nondecorated fibers on glass coverslips (Fig. 1D). When MDA-MB-231 cells were seeded for 15 min on this mixed, 2D network, we observed that the EGFR preferentially accumulated along EGF-decorated fibers as compared to nondecorated ones (Fig. 1, D and E). This preferential accumulation did not depend on EGFR activation as it was not significantly modulated by

Inserm U1279, Gustave Roussy Institute, Université Paris-Saclay, Villejuif, France.
*Corresponding author. Email: enzo.bresteau@gustaveroussy.fr (E.B.); guillaume.montagnac@gustaveroussy.fr (G.M.)
†Present address: Wolfson Wohl Cancer Research Centre, Institute of Cancer Sciences, University of Glasgow, Glasgow G61 1QH, UK.

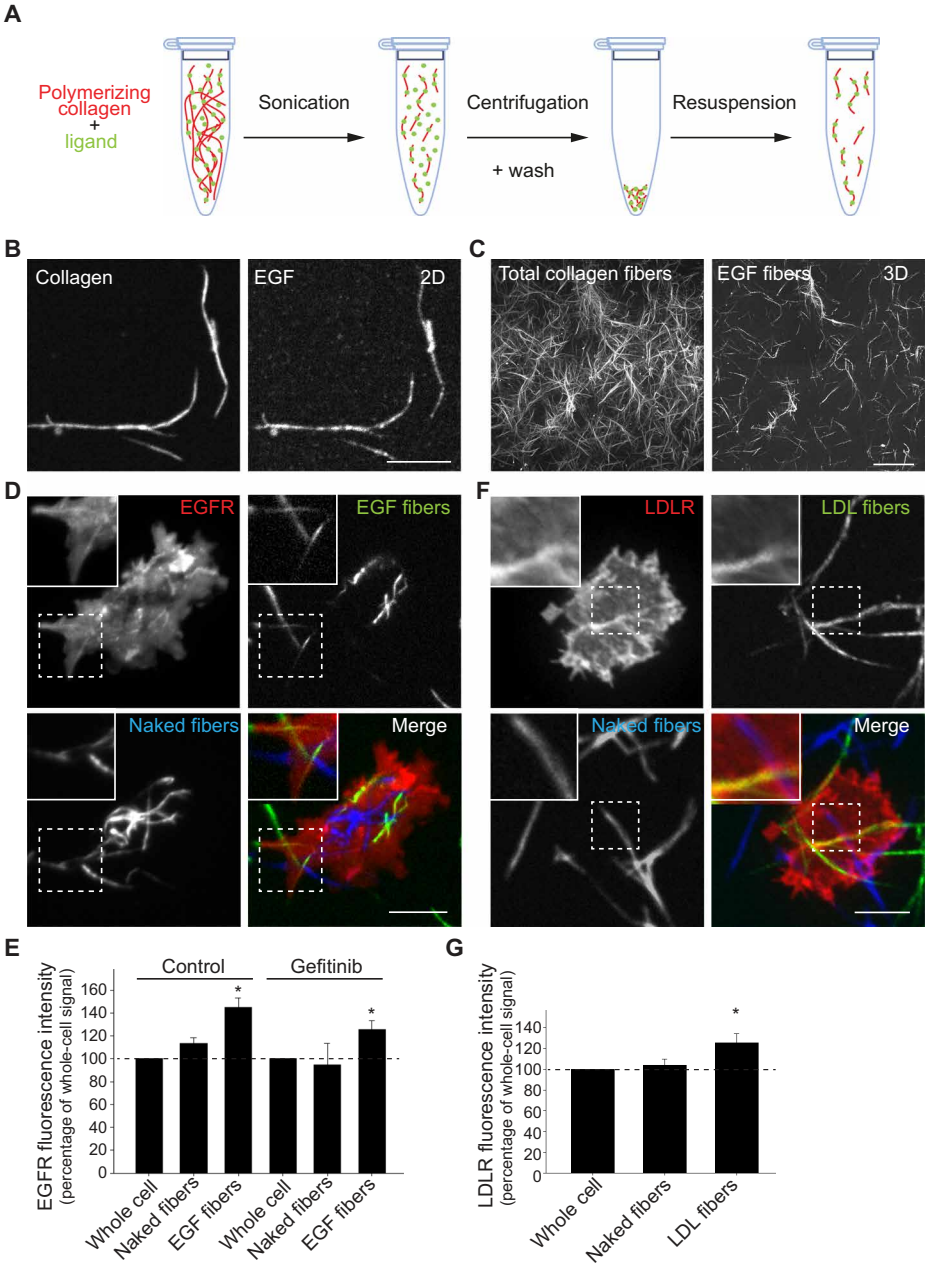

Fig. 1. Characterization of ligand-decorated collagen fibers. (**A**) Scheme representing the different steps of collagen fiber production and decoration with ligands. (**B**) Alexa548-labeled (left) and Alexa488-EGF–decorated (right) fibers produced as in (A) were spotted on a glass coverslip. Scale bar, 5 μm. (**C**) Alexa488-EGF–decorated fibers (right) produced as in (A) were embedded in a 3D collagen network (left). Scale bar, 20 μm. (**D**) MDA-MB-231 cells expressing GFP-tagged EGFR were allowed to spread on a composite network as in (D). Higher magnification of boxed area is shown. Scale bar, 10 μm. (**E**) Quantification of the enrichment of average GFP-EGFR fluorescence intensity on EGF-decorated fibers as compared to nondecorated fibers and to whole cell–associated fluorescence in MDA-MB-231 cells as in (D) and treated or not with gefitinib, as indicated. Data are expressed as the means ± SD of GFP fluorescence normalized to whole-cell fluorescence (*$P < 0.01$, one-way ANOVA; $N = 3$). (**F**) MDA-MB-231 cells expressing GFP-tagged LDLR were allowed to spread on a composite network composed of LDL-decorated and nondecorated fibers. Higher magnification of boxed area is shown. Scale bar, 10 μm. (**G**) Quantification of the enrichment of average GFP-LDLR fluorescence intensity on LDL-decorated fibers as compared to nondecorated fibers and to whole cell–associated fluorescence in MDA-MB-231 cells as in (F). Data are expressed as the means ± SD of GFP fluorescence normalized to whole-cell fluorescence (*$P < 0.01$, one-way ANOVA; $N = 3$).

treatment with gefitinib, a drug that inhibits the kinase activity of EGFR and thus abrogates the activation of downstream signaling pathways (Fig. 1E) (*12*). We also observed that the LDL receptor (LDLR) preferentially accumulated on LDL-decorated fibers (Fig. 1, F and G). Together, these data demonstrate that collagen fiber–associated ligands are functional and can be sensed by cells.

Preferential accumulation of TCALs along ligand-decorated fibers

Because local accumulation of receptors has been shown to trigger local accumulation of CCSs (*13*), we next stained cells seeded on the composite network for the α-adaptin subunit of the clathrin adaptor AP-2. We noticed that CCSs corresponding to previously described

TCALs (*4*) accumulated along nondecorated fibers but accumulated even more on Alexa488-EGF–decorated fibers (Fig. 2, A and B) or on heparin-binding (HB)–EGF (fig. S3A). We also observed a preferential accumulation of TCALs along Alexa488-EGF–decorated fibers when using MRC5 cells and immortalized primary cancer-associated fibroblasts (CAFs) or osteoblasts (fig. S3, B to D). Similar results were obtained when using unlabeled, native EGF (Fig. 2B). However, addition of soluble EGF prevented the preferential accumulation of TCALs along EGF-decorated fibers (fig. S3E), suggesting that EGFR occupation by soluble ligand prevents the cell to sense EGF on fibers.

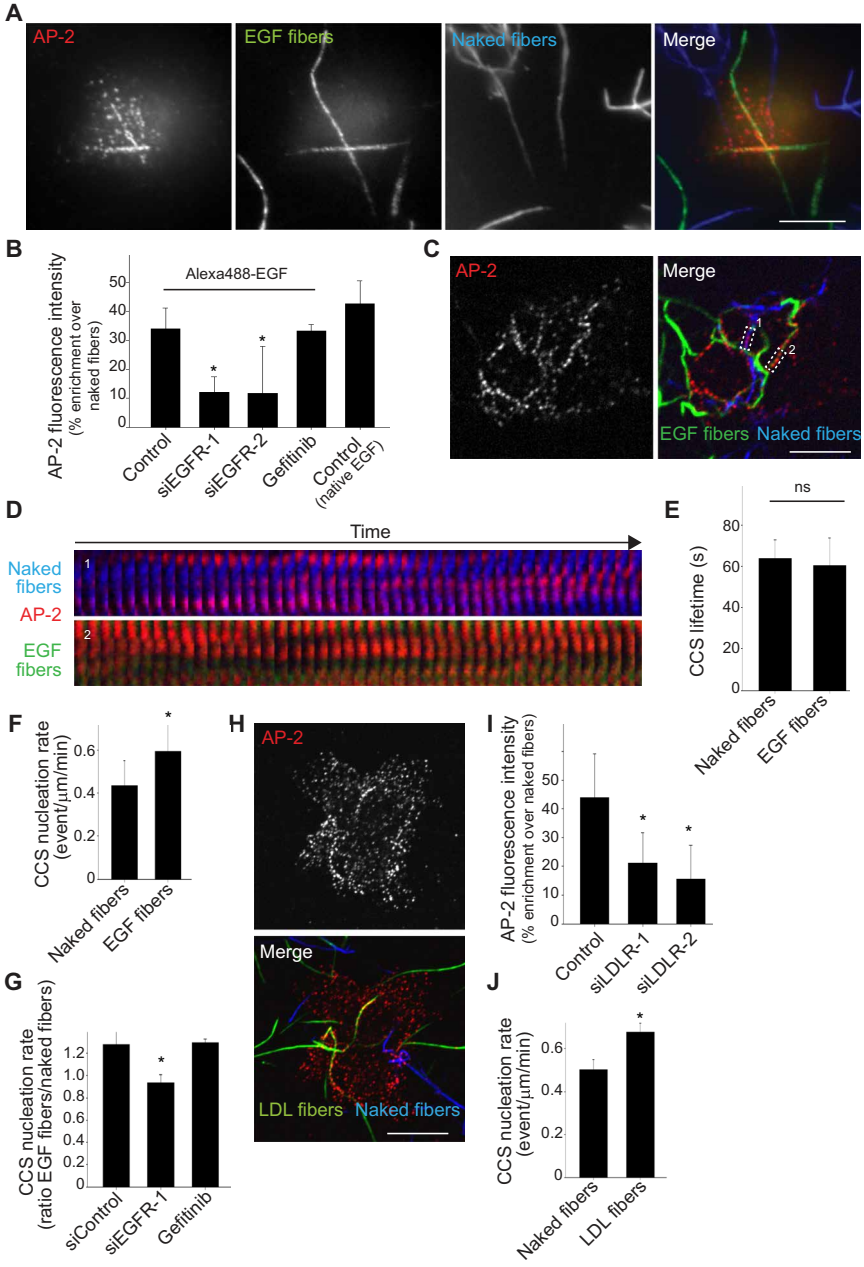

Fig. 2. TCALs preferentially accumulate along ligand-decorated fibers. (**A**) EGF-decorated (green) and naked (blue) fibers were spotted on a glass coverslip, and MDA-MB-231 cells were allowed to spread on this network for 15 min before being fixed and stained for α-adaptin (red). Scale bar, 10 μm. (**B**) Quantification of the enrichment of α-adaptin staining fluorescence intensity on indicated fibers as compared to naked fibers in cells as in (A) and treated with the indicated siRNA or with gefitinib (*$P < 0.01$, one-way ANOVA; $N = 3$). (**C**) Genome-edited MDA-MB-231 cells expressing mCherry-tagged μ2-adaptin (AP-2, red) were allowed to spread as in (A). Scale bar, 10 μm. (**D**) Kymographs of regions boxed in (C) over a 2-min time period. (**E** and **F**) Quantification of the lifetime (E) or nucleation rate (F) of CCSs located on indicated fibers (*$P < 0.01$, Student's *t* test; $N = 3$). (**G**) Quantification of the ratio of CCS nucleation rate on EGF-decorated versus naked fibers in cells treated with the indicated siRNA or with gefitinib (*$P < 0.001$, one-way ANOVA; $N = 3$). (**H**) Dil-LDL–decorated fibers (green) and naked fibers (blue) were spotted on a glass coverslip, and MDA-MB-231 cells were allowed to spread on this network for 15 min before being fixed and stained for α-adaptin (red). Scale bar, 10 μm. (**I**) Quantification of the enrichment of average α-adaptin staining fluorescence intensity on Dil-LDL–decorated as compared to naked fibers (*$P < 0.01$, Student's *t* test; $N = 3$). (**J**) Quantification of the average nucleation rate of CCSs located on indicated fibers (*$P < 0.01$, Student's *t* test; $N = 3$). All results are expressed as means ± SD. ns, not significant.

The preferential accumulation of TCALs along EGF-decorated fibers was dependent on the expression of the EGFR but not on its signaling activity (Fig. 2B and fig. S3C). We controlled that gefitinib was able to inhibit EGF-induced Erk activation (fig. S3F). These results suggest that EGFR activation and downstream signaling pathways are not playing a role in the preferential accumulation of TCALs along EGF-decorated fibers.

We next performed live-cell imaging of genome-edited MDA-MB-231 cells engineered to express green fluorescent protein (GFP)–tagged, endogenous μ2-adaptin subunit of AP-2. When these cells were allowed to spread for 15 min on the composite, 2D network, we measured that TCAL average lifetime was similar for EGF-decorated and nondecorated fibers (Fig. 2, C to E, and movie S1). However, the nucleation rate of TCALs on EGF-decorated fibers was increased by approximately 30% as compared to control fibers (Fig. 2, F and G). EGFR knockdown, but not gefitinib treatment, reduced TCAL nucleation rate on EGF-decorated fibers to the level observed on nondecorated fibers (Fig. 2G). It has been suggested that, in particular experimental setups, EGF/EGFR complexes could induce the de novo formation of CCSs (*14*, *15*). In addition, receptors are known to take an important part in the maturation of nascent CCSs (*16*, *17*), and experimental clustering of cell surface receptors can induce the de novo formation of CCSs (*13*). Thus, it is possible that local accumulation of EGFR driven by collagen fiber–associated EGF facilitates local TCAL nucleation/maturation, as suggested by our data. The role of EGFR kinase activity in EGFR interaction with CCSs has been supported by several studies (*18*, *19*), but some others suggested that EGF-induced receptor dimerization is sufficient to be recruited at CCSs (*20*, *21*). In any case, our results suggest that EGF/EGFR-regulated local TCAL nucleation does not require EGFR activation. Along this line, we observed that EGF still accumulates at CCSs in cells seeded on glass and treated with gefitinib, although less efficiently than in control cells (fig. S3, G and H). It is possible that the particular conditions of TCAL assembly, which we previously showed to be driven by cooperation between local membrane curvature and β_1-integrin engagement (*4*), are further favored by high local concentrations of functional CCS cargoes. In agreement with that, we observed that TCALs also preferentially accumulated along Dil-LDL–decorated fibers as compared to nondecorated ones not only in MDA-MB-231 cells but also in MRC5 cells and in primary osteoblasts (Fig. 2, H and I, and fig. S3, C and D). In addition, this preferential accumulation depended on the expression of the LDLR (Fig. 2I and fig. S3C). Because the LDLR is not known to elicit downstream signaling events (*22*), these data further confirm that local CCS ligand accumulation on collagen fibers results in the accumulation of TCALs independently of ligand-triggered signaling pathways. Similar to EGF-decorated fibers, TCAL nucleation rate was increased on LDL-decorated fibers as compared to nondecorated ones (Fig. 2J). Thus, local accumulation of CCS ligands on collagen fibers drives the local accumulation of TCALs through increasing their nucleation rate.

Local TCAL accumulation regulates local forces applied on collagen fibers

We noticed that cells spreading on the mixed 2D network developed longer protrusions along EGF-decorated fibers as compared to nondecorated fibers (Fig. 3, A and B). This correlated with increased protrusion speed on these types of fibers (fig. S4A). However, we did not observe any differential enrichment of β_1-integrin on one or the other type of fiber (fig. S4, B and C). This suggests that, although β_1-integrin is required for TCAL accumulation on collagen fibers (*4*), the increased accumulation of TCALs along EGF-decorated fibers does not require an increased recruitment of β_1-integrin. In addition, the focal adhesion marker vinculin was equally distributed between EGF-decorated and nondecorated fibers (fig. S4, D and E), suggesting that these adhesion structures do not regulate the differential protrusion activity on the two different types of fibers. Also, active myosin-II did not particularly associate with either fiber type (fig. S4, F and G). However, knockdown of the EGFR or the AP-2 subunit α-adaptin abrogated the differential protrusion potential between EGF-decorated and nondecorated fibers (Fig. 3B). Notably, addition of soluble EGF also abolished the preferential protrusion activity along EGF-decorated fibers (fig. S4H). However, gefitinib treatment did not modulate the preferential protrusion activity on EGF-decorated fibers (fig. S4H). Notably, cells also preferentially established their main protrusion in association with HB-EGF–decorated fibers rather than with naked fibers (fig. S4H). We previously reported that TCALs help cells to develop long protrusions in 3D collagen networks by providing several anchoring points to collagen fibers (*4*). Here, our data suggest that the increased accumulation of TCALs along EGF-decorated fibers allows the cell to develop longer protrusions on these fibers as compared to nondecorated fibers. Notably, cells also preferentially protruded along LDL-decorated fibers (fig. S4, I and J). Together, our data suggest that a local, increased accumulation of TCALs on some fibers drives the local formation of long protrusions on these fibers.

The increased protrusive activity on ligand-decorated fibers suggested that cells may exert more forces on these fibers. To test this hypothesis, we first performed traction force microscopy assays on polyacrylamide gels on which both EGF-decorated and nondecorated fibers were spotted. We observed that MDA-MB-231 cells seemed to exert more forces on EGF-decorated fibers as compared to naked fibers (Fig. 3C). To better quantify this, we next used traction force gels on which only EGF-decorated or only naked fibers were spotted (fig. S5A) and measured that MDA-MB-231 cells exerted significantly more forces on EGF-decorated fibers (Fig. 3D). Similar results were obtained with cells treated with gefitinib, indicating that EGFR activation is not required for cells to exert more forces on EGF-decorated fibers (Fig. 3D). MDA-MB-231 cells also significantly exerted more forces on gels coated with LDL-decorated fibers (fig. S5B). To further test whether more forces are specifically applied on EGF-decorated fibers as compared to nondecorated ones, we aimed at developing a collagen fiber remodeling assay. We first observed that MDA-MB-231 cells seeded on fiber-coated glass remodeled collagen fibers through pulling on them before packing them on their dorsal surface in a myosin-II activity–dependent manner (Fig. 3, E and F). In the course of this process, TCALs were observed colocalizing and moving together with collagen fibers on the dorsal surface of cells (fig. S5, C and D). CCSs were already shown to move laterally at the plasma membrane and, more specifically, to be dragged by the acto-myosin retrograde flow at the cell leading edge (*23*, *24*). We confirmed that CCSs located at the leading edge of MDA-MB-231 cells experience retrograde movements that correlate with acto-myosin retrograde flow (fig. S5, E and F). Moreover, inhibition of myosin-II–regulated actin retrograde flow in the lamella abrogated CCS retrograde movements (fig. S5, F and G). These data suggest that TCALs could be used to transmit acto-myosin–generated forces onto collagen fibers.

To test this hypothesis and further analyze the specificity of force transmission to ligand-decorated fibers, we next used composite

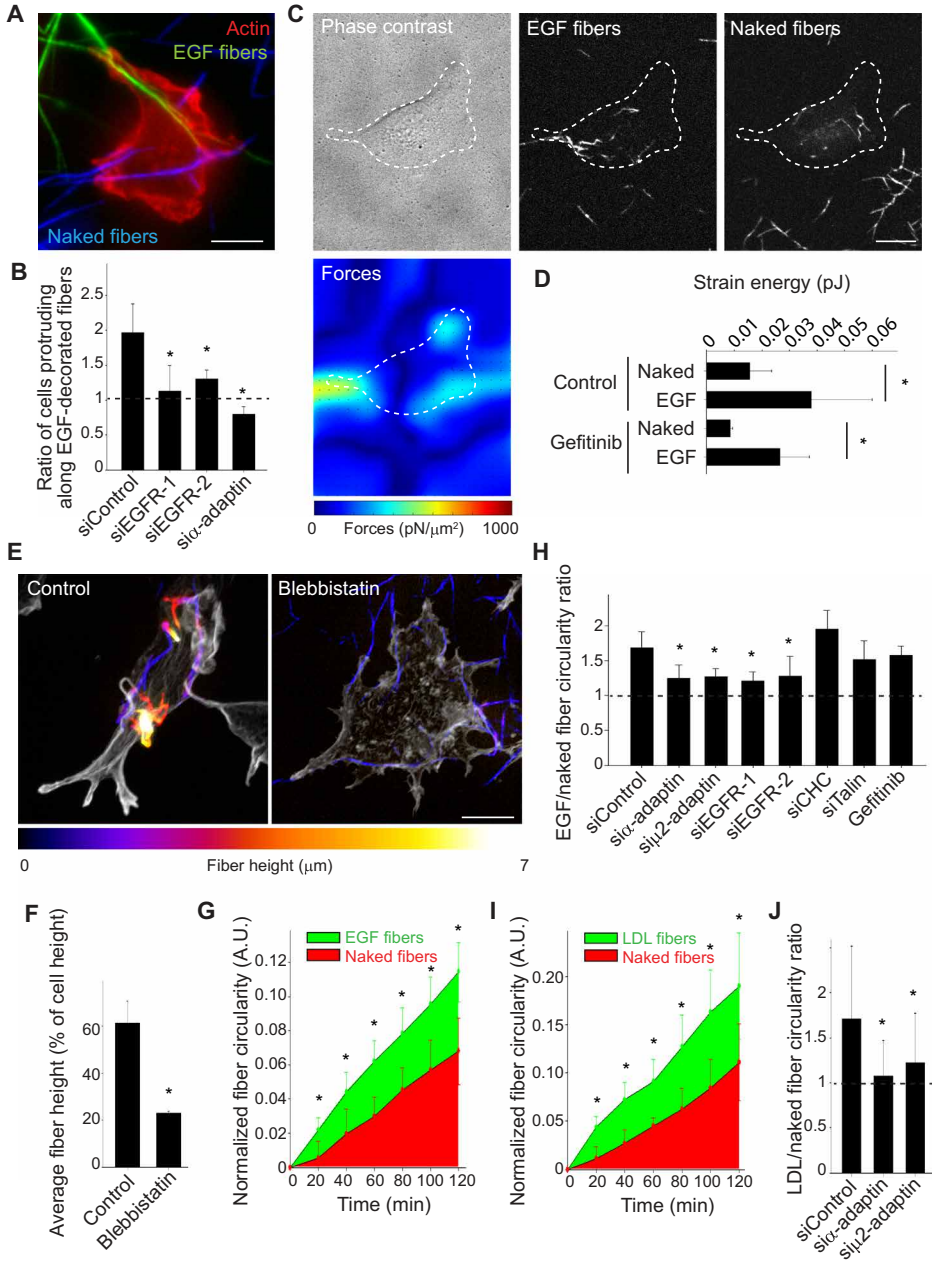

Fig. 3. TCALs allow cells to preferentially remodel ligand-decorated fibers. (**A**) MDA-MB-231 cells were allowed to spread for 20 min on a glass coverslip spotted with EGF-decorated and naked fibers before being fixed and stained with phalloidin. Scale bar, 10 μm. (**B**) Quantification of the ratio of cells developing their longest protrusion along EGF-decorated versus naked fibers in cells treated with the indicated siRNAs (*$P < 0.01$, one-way ANOVA; $N = 3$). (**C**) Representative images of MDA-MB-231 cells, fibers, and traction force map on 5-kPa polyacrylamide gels spotted with naked and EGF-decorated fibers. Scale bar, 10 μm. Dashed lines represent cell contours. Color code gives the magnitude of traction stress in piconewton per square micrometer. (**D**) Average strain energy exerted by cells on gels spotted with naked or EGF-decorated fibers and treated or not with gefitinib (*$P < 0.01$, Student's t test; $N = 3$). (**E**) Maximum z-stack projections of control or blebbistatin-treated MDA-MB-231 cells allowed to remodel naked fibers for 90 min. Fibers were color coded according to their position in the z-stack. (**F**) Quantification of the height of fibers expressed in percentage of cell height. (**G** and **I**) Quantification of the average evolution of EGF-decorated (G) or LDL-decorated (I) and naked fiber circularity upon cell seeding on a composite, 2D network (*$P < 0.01$, one-way ANOVA; $N = 3$). (**H** and **J**) Quantification of the ratio of EGF-decorated (H) or LDL-decorated (J) versus naked fiber circularity at $t = 120$ min in cells treated with indicated siRNAs or with gefitinib (*$P < 0.001$, one-way ANOVA; $N = 3$). All results are expressed as means ± SD. A.U., arbitrary units.

substrates through sequentially spotting EGF-decorated and non-decorated fibers on a glass coverslip. MDA-MB-231 cells were seeded on and allowed to remodel this composite network for 2 hours. Collagen fiber remodeling was characterized by a transition from rod-like bundles to globular aggregates as cells pulled on and progressively packed fibers on their dorsal surface (movie S2). We noticed that EGF-decorated fibers seemed to have been remodeled faster than non-decorated fibers (fig. S6, A and B, and movie S2). To more precisely quantify fiber remodeling, we measured the evolution of fiber circularity over time. The data show that EGF-decorated fibers were more

remodeled as compared to nondecorated fibers (Fig. 3, G and H). Similar results were obtained when using MRC5 cells, CAFs, and osteoblasts (fig. S6C). Notably, EGF-decorated fibers were similarly remodeled by MDA-MB-231 cells, whether presented alone or mixed in a 1:1 ratio with naked fibers (fig. S6D). However, naked fibers seemed more remodeled when presented alone than when mixed with EGF-decorated fibers, although this was not statistically significant (fig. S6D). This suggests that the ratio of decorated versus nondecorated fibers does not deeply affect the preferential remodeling. The preferential remodeling of EGF-decorated fibers was dependent on EGFR expression (Fig. 3H and fig. S6E). However, gefitinib treatment did not modulate the preferential remodeling of EGF-decorated fibers, indicating that EGFR signaling is not required (Fig. 3H and fig. S6E). Knockdown of AP-2 subunits abrogated the preferential remodeling of collagen fibers (Fig. 3H and fig. S6E). Notably, although TCALs accumulated even more on EGF-decorated fibers upon clathrin knockdown (fig. S6F), EGF-decorated fibers were only slightly, but not significantly, preferentially more remodeled under these conditions (Fig. 3H and fig. S6E). This is consistent with our previous characterization of TCALs, showing that clathrin is not required for the accumulation of AP-2–positive structures along collagen fibers and that it does not play a role in the adhesive function of TCALs (*4*). Because clathrin is required for CCS budding, this also indicates that the preferential remodeling phenotype does not depend on endocytosis. Notably, inhibiting the formation of focal adhesions by using Talin-specific small interfering RNAs (siRNAs) strongly reduced the remodeling rates of the two fiber types but did not inhibit the preferential remodeling of EGF-decorated fibers (Fig. 3H and fig. S6E). Together, our data show that both EGFR and TCALs are required for the preferential remodeling of EGF-decorated collagen fibers. In addition, we observed that LDL-decorated fibers were also preferentially remodeled over nondecorated fibers and that this also depended on AP-2 (Fig. 3, I and J). Thus, our data suggest that the increased accumulation of TCALs along CCS ligand–decorated fibers leads to an increased local force transmission in a very specific manner as cells simultaneously contact both decorated and nondecorated fibers in our assay.

Local TCAL accumulation steers cell migration in 3D

We previously reported that TCALs help cells migrate in 3D environments by serving as adhesion structures to collagen fibers (*4*). We hypothesized that the preferential accumulation of TCALs along ligand-decorated fibers could further favor cell migration in 3D networks. We first observed that MDA-MB-231 cells located in a 3D network composed of EGF-decorated fibers were more elongated as compared to cells evolving in a nondecorated network (Fig. 4, A and B). This increased spreading in the EGF-decorated network depended on both EGFR and AP-2 (Fig. 4B). Together with our previous results showing that TCALs help cells build long protrusions required for migration (*4*), these data suggested that EGF on collagen fibers may potentiate cell elongation through favoring TCAL formation. However, cells migrated with a similar velocity in the EGF-decorated and nondecorated networks (fig. S7A). We controlled that EGF or LDL bound to collagen fibers did not modulate the average pore size of 3D gels (5.67 ± 0.08 μm for control gels; 5.57 ± 0.23 and 5.7 ± 0.6 μm for gels composed of EGF-decorated or LDL-decorated collagen fibers, respectively). However, cells migrated significantly faster in our gels as compared to collagen gels polymerized according to classical protocols (fig. S7A), probably reflecting a differential degree of interconnection between fibers. However, cell proliferation was similar in both networks (fig. S7B). It is possible that a homogeneous distribution of EGF-decorated fibers around the cell leads to a global stabilization of all cellular protrusions, without a net consequence on cell displacement in one given direction. To circumvent this potential issue, we generated a composite 3D network in which EGF-decorated fibers are restricted to a defined area of the gel (see movie S3 and Materials and Methods). We controlled that EGF-decorated fibers were clearly segregated from nondecorated fibers and that no physical boundary between the two regions could be detected (Fig. 4C). The interface between EGF-decorated and nondecorated areas was stable for at least 24 hours (fig. S7C). We observed that cells located in homogeneously EGF-decorated or nondecorated areas of the gel migrated randomly in all directions (Fig. 4D). However, when considering cells located at the border between the two areas or coming into contact with this border during the acquisition period and tracking them from this starting point, we observed that they preferentially migrated toward the EGF-decorated network (Fig. 4, D and E). We controlled that our setup does not intrinsically bias the direction of migration, as cells tracked from the border of a composite gel composed of two nondecorated fiber–containing networks migrated randomly toward both areas (fig. S7D). The preferential migration toward EGF-decorated fibers was dependent on EGFR and AP-2 (Fig. 4E). We obtained similar results when using MRC5 cells (fig. S7E). In addition, we were also able to produce a composite 3D network with a clear segregation between LDL-decorated and nondecorated fibers (fig. S7F). Similar to the results obtained above with EGF-decorated fibers, cells preferentially migrated toward LDL-decorated fibers in an AP-2– and LDLR-dependent manner (Fig. 4F). Together, our results suggest that TCAL accumulation on CCS ligand–decorated fibers allows cells to migrate toward this type of fiber.

Overall, we have found that TCALs strongly accumulate on CCS ligand–decorated fibers because ligand/receptor complexes favor the local nucleation of TCALs on these fibers. The preferential accumulation of TCALs on ligand-decorated fibers allows the cell to exert more forces on these fibers as compared to nondecorated fibers. As a consequence, cells preferentially migrate toward ligand-decorated fibers in 3D environments. Notably, this directed mode of migration does not depend on the transduction of signaling pathways but only on the local accumulation of TCALs that allows cells to pull stronger on collagen fibers decorated with CCS ligands. Because ECM fibers are abundant in complex organisms and many chemoattractants and other potential CCS ligands are known to bind to ECM, the mechanism we described here may play a central role in cell migration in different contexts, from development to cancers.

MATERIALS AND METHODS

Cell lines

MDA-MB-231 cells (a gift from P. Chavrier, Institut Curie, Paris, France), genome-edited MDA-MB-231 cells engineered to express an endogenous GFP-tagged or mCherry-tagged μ2 subunit (a gift from D. Drubin, University of California, Berkeley, Berkeley, CA, USA), MRC5 cells, immortalized human colon CAFs (a gift from D. Vignjevic, Institut Curie, Paris, France), and immortalized mouse osteoblasts (a gift from C. Albiges-Rizo, IAB, Grenoble, France) were grown in Dulbecco's modified Eagle's medium (DMEM) Glutamax (Gibco) supplemented with 10% fetal calf serum (FCS; Gibco) at 37°C in 5% CO_2.

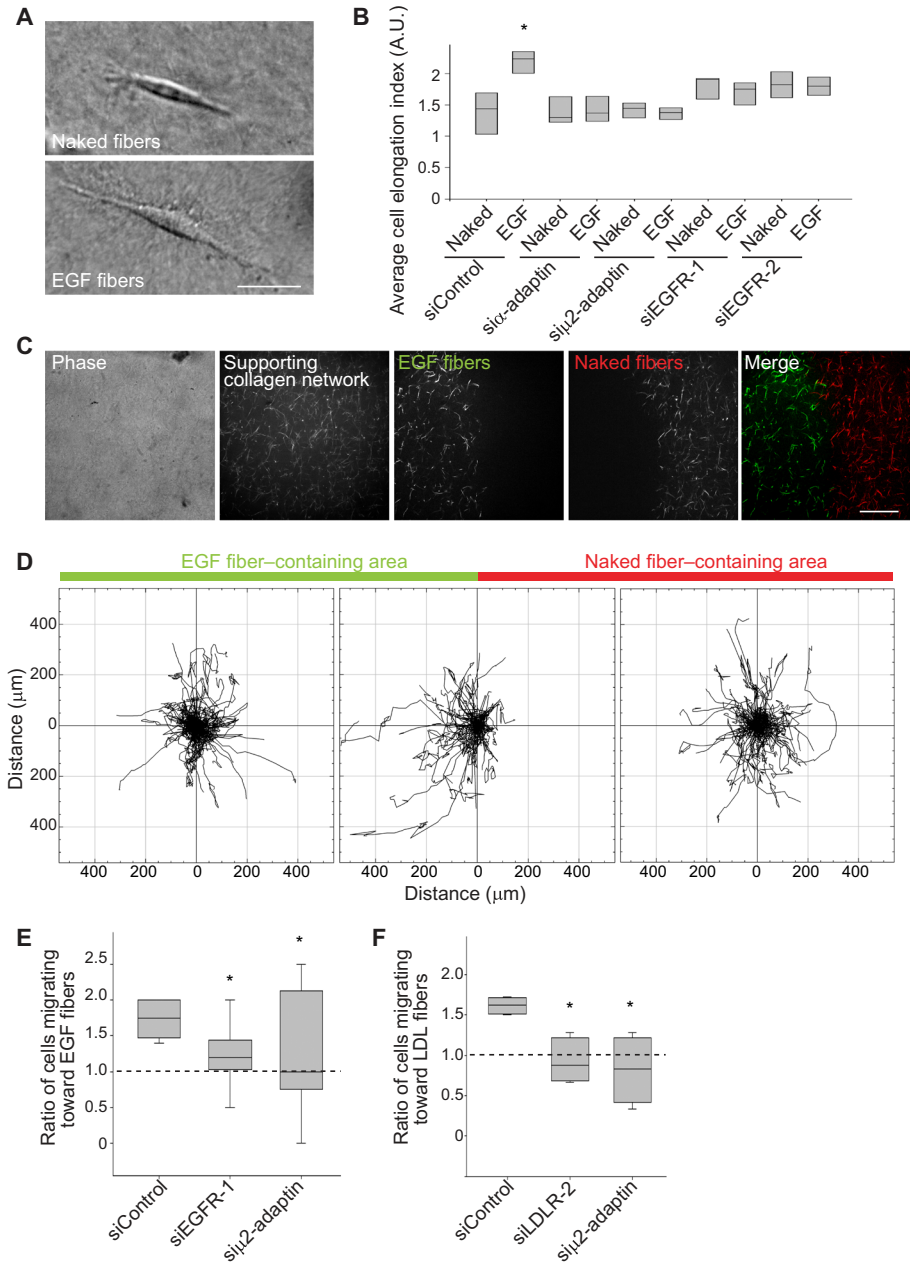

Fig. 4. TCALs regulate 3D directed migration toward EGF-decorated fibers. (**A**) MDA-MB-231 cells were embedded in nondecorated fiber–corated fi (top) or in EGF-decorated fiber-–or in EGF (bottom) 3D collagen network and imaged 24 hours later (representative images of three independent experiments). Scale bar, 10 μm. (**B**) Quantification of the means ± SD elongation index of cells embedded in naked fiber-– elongati or EGF fiber–containing 3D networks, as indicated (*$P < 0.01$, one-way ANOVA; $N = 3$). (**C**) Engineered composite 3D network comprising a nondecorated fiber (naked, red)–containing area and an EGF-decorated fiber (green)–containing area in a supporting collagen gel was imaged by spinning disk microscopy. A phase-contrast image of the same region of the composite network is shown. Scale bar, 20 μm. (**D**) Track plots representing the tracks of individual migrating MDA-MB-231 cells located in the EGF fiber–containing area (left), the nondecorated fiber–containing area (right), or at the border between the two areas (middle). (**E**) Box plots representing the average ratio of cells initially located at the border between the two areas as depicted in (C) and migrating toward the EGF fiber–containing area versus the nondecorated fiber area SD (*$P < 0.001$, one-way ANOVA). A ratio of 1 indicates no preferential migration toward one or the other area. (**F**) Box plots representing the average ratio of cells initially located at the border between the nondecorated and LDL-decorated areas and migrating toward the LDL fiber–containing area versus the nondecorated fiber area SD (*$P < 0.001$, one-way ANOVA). A ratio of 1 indicates no preferential migration toward one or the other area.

Antibodies, growth factors, and drugs

Anti-vinculin antibodies were a gift from D. Vignjevic (Institut Curie, France). Rabbit polyclonal anti–α-adaptin antibodies were purchased from Santa Cruz Biotechnology Inc. Mouse monoclonal anti–α-adaptin antibodies were purchased from Abcam. Activated integrin (4B4) antibody was purchased from Beckman Coulter. Alexa488-conjugated anti-mouse or anti-rabbit antibodies and Alexa546- or Alexa488-labeled phalloidin were purchased from Molecular Probes. Anti-Erk1/2 and anti–phospho-Erk1/2 antibodies were purchased from Cell Signaling Technology. Horseradish peroxidase (HRP)–conjugated

anti-mouse antibodies for Western blot and Cy3-conjugated anti-rabbit or anti-mouse antibodies were purchased from Jackson ImmunoResearch Laboratories. HRP-conjugated anti-rabbit antibodies for Western blot were purchased from Sigma-Aldrich. Gefitinib and blebbistatin were purchased from Sigma-Aldrich and used at a final concentration of 10 μM unless otherwise stated. Before the experiment, cells with gefitinib/blebbistatin were pretreated for 30 min at 37°C. Alexa Fluor 488– or Alexa Fluor 647–labeled EGF and Dil-conjugated LDL were purchased from Thermo Fisher Scientific. Rat tail collagen-I was purchased from Gibco. Human recombinant EGF was purchased from Sigma-Aldrich. Penicillin-streptomycin was purchased from Thermo Fisher Scientific and used at a final concentration of 100 U/ml.

RNA interference

For siRNA depletion, MDA-MB-231 cells were plated at 50% confluence and treated with the indicated siRNA (30 nM) using RNAiMAX (Invitrogen) according to the manufacturer's instruction. Cells were used upon optimal protein depletion after 72 or 120 hours (when using two rounds of siRNA transfection) of siRNA treatment as shown by immunoblotting analysis with specific antibodies. Equal loading of the cell lysates was verified by immunoblotting with anti-tubulin antibodies. The following siRNAs were used: Talin, 5′-ACAAGAUGGAUGAAUCAAUUUU-3′; μ2-adaptin, 5′-AAGUGGAUGCCUUUCGGGUCA-3′; clathrin heavy chain, 5′-GCUGGGAAAACUCUUCAGATT-3′; α-adaptin, 5′-AUGGCGGUGGUGUCGGCUCTT-3′; EGFR, 5′-GAGGAAAUAUGUACUACGA-3′ (EGFR-1) and 5′-GCAAAGUGUGUAACGGAAUAGGUAU-3′ (EGFR-2); LDLR, 5′-GGACAGAUAUCAUCAACGA-3′ (LDLR-1) and 5′-UCGUUGAUGAUAUCUGUCC-3′ (LDLR-2); nontargeting siRNAs (siControl), ON-TARGETplus nontargeting SMARTpool siRNAs.

Western blots

For Western blot experiments, cells were lysed in ice-cold MAPK buffer [100 mM NaCl, 10 nM EDTA, 1% IGEPAL CA-630, 0.1% SDS, and 50 mM tris-HCl (pH 7.4)] supplemented with protease and phosphatase inhibitors. Antibodies were diluted at 1:1000 in phosphate-buffered saline (PBS)–0.1% Tween–5% bovine serum albumin or 5% nonfat dried milk. Analyses of band densitometry were performed using ImageJ.

For testing gefitinib-mediated inhibition of EGFR signaling, 200,000 MDA-MB-231 cells were serum starved for 2 hours and then stimulated or not with EGF (10 ng/ml) in the presence or not of 10 μM gefitinib for 5 min at 37°C. Cells were then harvested, lysed, and analyzed by Western blot as describe above.

EGF/LDL-decorated collagen fibers and 3D networks

A mix (200 μl) containing a 10:1 ratio of unlabeled collagen type I and Alexa548 (or Alexa488 or Alexa647)–labeled collagen type I (Gibco) at a final concentration of 1.1 mg/ml was allowed to polymerize in a 1.5-ml Protein LoBind tube (Eppendorf) for 12 min at room temperature (RT). PBS (200 μl) on ice was then added to the mix before three rounds of 10-s sonication were performed using a Q125 sonicator at 40% amplitude (Qsonica sonication). EGF or LDL (2.5 μl) was then added (or not) to the mix before incubation at RT for 2.5 hours (final concentration for EGF, 1.25 μg/ml and for LDL, 6.25 mg/ml). PBS (600 μl) was then added to the mix before 12 rounds of 10-s sonication were performed at 40% amplitude. Polymerized, sonicated, EGF- or LDL- or nondecorated collagen fibers were then pelleted by centrifugation for 1 hour at 4500 rpm at 4°C. The pellet was washed twice with cold PBS before being either resuspended in 1 ml of cold PBS (for coverslip spotting experiments) or incorporated into another mix for 3D collagen network preparation. Fiber solution was kept on ice to prevent collagen fiber aggregation.

For collagen fiber spotting on glass coverslips (2D), 100 μl of the mix containing polymerized, sonicated collagen fibers was spotted for 10 min on a 12-mm glass coverslip or in a glass-bottom 96-well plate (Greiner) at RT before being washed twice with PBS. For sequential deposition experiments, naked fibers were spotted as described, then washed twice with PBS before EGF- or LDL-decorated fibers were spotted for 10 min as well, and washed twice using PBS.

For incorporation into 3D networks, the pellet composed of polymerized, sonicated collagen fibers was resuspended in a 200-μl mix containing Alexa-labeled or unlabeled, nonpolymerized collagen I at 1.1 mg/ml, and 45 μl of this new mix was deposited in a glass-bottom 96-well plate pretreated with 0.1% poly-L-lysin (Sigma-Aldrich) for 10 min. For some experiments, the mix contained 300 cells/μl. The mix was allowed to polymerize at RT for 30 min before being covered with complete medium supplemented with penicillin-streptomycin. For generating composite 3D networks, 7 μl of a mix containing EGF- or LDL-decorated, polymerized, and sonicated fibers and 300 cells/μl was gently pipetted inside a 45-μl mix containing naked, polymerized, sonicated fibers and 300 cells/μl that was deposited on glass a few seconds before. The composite 3D network was then allowed to polymerize at RT for 30 min before being covered with complete medium supplemented with penicillin-streptomycin. To characterize the interface in composite networks, the 3D gels were imaged at ×100 using the spinning disk microscope described below, and z-stack of 26 μm was acquired with one image every micrometer.

Indirect immunofluorescence microscopy and fluorescence quantification

Control or siRNA-treated MDA-MB-231 cells plated for 15 min on top of naked and EGF- or LDL-decorated fibers spotted on coverslips were fixed in ice-cold methanol or paraformaldehyde (PFA) and processed for immunofluorescence microscopy by using the indicated antibodies. Cells were imaged through a 100× 1.40 numerical aperture (NA) UPlanSApo objective lens of a wide-field IX73 microscope (Olympus) equipped with an Orca-Flash2.8 complementary metal-oxide semiconductor (CMOS) camera (Hamamatsu) and steered by CellSens Dimension software (Olympus).

For calculating the degree of CCS, integrin, or vinculin accumulation along collagen fibers, naked and decorated fibers were segmented using ImageJ software, and the average fluorescence intensity of the anti–α-adaptin, anti-integrin, or anti-vinculin staining in fiber area was measured for both types of fibers and for each individual cell and normalized to the area occupied by respective collagen fibers. For protrusion quantification, individual cells were ranked on the basis of the association of their main protrusion with either EGF-decorated, LDL-decorated, or naked fibers. At least 50 cells per condition were quantified in three to five independent experiments.

Total internal reflection fluorescence microscopy

For total internal reflection fluorescence (TIRF) microscopy, MDA-MB-231 cells seeded on glass or onto collagen fiber–coated glass coverslips were imaged through a 100× 1.49 NA TIRF objective lens on a Nikon TE2000 (Nikon France SAS, Champigny sur Marne, France) inverted microscope equipped with a QuantEM EMCCD camera (Roper Scientific SAS, Evry, France/Photometrics, AZ, USA), a dual-output laser launch, which included 491- and 561-nm 50-mW DPSS

lasers (Roper Scientific), and driven by Metamorph 7 software (MDS Analytical Technologies, Sunnyvale, CA, USA). A motorized device driven by Metamorph allowed the accurate positioning of the illumination light for evanescent wave excitation.

To measure EGFR or LDLR accumulation on collagen fibers, MDA-MB-231 cells were transfected with an EGFR-GFP (a gift from A. Sorkin from the University of Pittsburg, USA) or LDLR-GFP (a gift from C. Almeida from Institut Curie, France) encoding plasmid. Plasmids were transfected 24 hours after cell plating using polyethylenimine (PEI; MW 25.000, Polysciences) at 1 mg/ml according to the following protocol: 2 μg of DNA was added to 100 μl of Opti-MEM, followed by addition of 4 μl of PEI, vortex, and incubation for 10 min at RT before adding the mix to the cells. Gefitinib-treated or untreated cells were allowed to spread for approximately 15 min on top of a mixed network composed of naked and EGF- or LDL-decorated fibers spotted onto a glass-bottom FluoroDish (World Precision Instruments) before being imaged for 5 min. EGFR- or LDLR-associated average fluorescence intensity was quantified in ImageJ using the above-described segmentation protocol at time points showing the greatest accumulation of EGFR or LDLR on fibers. At least 15 cells per condition were analyzed in two to three independent experiments.

To monitor EGF recruitment at CCSs, genome-edited MDA-MB-231 cells on FluoroDishes were starved for 2 hours and treated or not with 10 mM gefitinib for 30 min before being incubated in the presence of the same concentration of gefitinib and Alexa488-EGF (50 ng/ml) before being imaged for 10 min. For quantification, CCSs were individually segmented using ImageJ, and average EGF-associated fluorescence was measured at the time point showing the maximum colocalization between EGF and CCSs. At least 2000 CCSs from at least five cells per condition and per experiment were quantified in two independent experiments.

Fluorescence recovery after photobleaching

EGF-decorated collagen fibers were spotted on glass or embedded in a 3D gel as described above in the presence or not of Alexa488-EGF (8 μg/ml). FRAP was performed on a Leica Sp8 confocal microscope equipped with a Pecon incubation chamber to maintain the cells at 37°C and 5% CO_2 and using the FRAP wizard of the Leica software. One fiber was manually selected and subjected to 100% laser power. One frame was collected before photobleaching, and 40 frames were collected after bleaching to analyze fluorescent recovery at a frequency of 1 frame/30 s. Data were analyzed using the ImageJ FRAP Profiler plugin (McMaster University, Canada) to extract recovery curves and calculate the half-time recovery. Three independent experiments were quantified.

Fiber-associated EGF stimulation and internalization assays

For fiber-associated EGF stimulation assays, MDA-MB-231 cells were starved for 6 hours before being harvested using trypsin and incubated in suspension alone or in the presence of Alexa-488 EGF, or naked fibers, or Alexa488-EGF–decorated fibers (50 ng/ml), as indicated. The amount of fibers used in the assay was chosen so that the concentration of Alexa488-EGF on EGF-decorated fibers was equivalent to soluble EGF (50 ng/ml) as determined by measuring Alexa488-EGF fluorescence on decorated fibers using a FLUOstar OPTIMA microplate reader. Cells were incubated at 37°C for 5 or 30 min before cells were harvested at 4°C and subjected to lysis in cold MAPK buffer followed by Western blot analyses using the indicated antibodies.

For fiber-associated EGF internalization assays, cells were incubated for 5, 10, 20, or 40 min on a coverslip coated with Alexa548-conjugated collagen fibers decorated with Alexa488-EGF. Cells were fixed with PFA and imaged by epifluorescence microscopy. Fluorescence was measured from both inside the cells and EGF-decorated fibers below the cells using ImageJ software. At least 20 cells per condition and per experiment were analyzed in three independent experiments.

Spinning disk microscopy

Following procedures previously described by Baschieri *et al.* (*25*), control or siRNA-treated, genome-edited MDA-MB-231 cells were imaged for exposure times of 200 ms at 5-s intervals for the indicated time using a spinning disk microscope (Andor) based on a CSU-W1 Yokogawa head mounted on the lateral port of an inverted IX-83 Olympus microscope equipped with a 60× 1.35 NA UPLSAPO objective lens and a laser combiner system, which included 491- and 561-nm 100-mW DPSS lasers (Andor). Images were acquired with a Zyla sCMOS camera (Andor). Alternatively, cells were imaged on a Nikon Ti2 Eclipse (Nikon France SAS, Champigny sur Marne, France) inverted microscope equipped with a 60× 1.40 NA oil objective (WD 0.130), a sCMOS PRIME 95B camera (Photometrics, AZ, USA), and a dual-output laser launch, which included 405-, 488-, 561-, and 642-nm 30-mW lasers. The emission filter characteristics are as follows: 452/45 nm (Semrock Part# FF01-452/45), 470/24 nm (Chroma 348716), 525/50 nm (Semrock Part# FF03-525/50), 545/40 nm (Chroma 346986), 609/54 nm (Semrock Part# FF01-609/54), and 708/75 nm (Semrock Part# FF01 708/75). Both microscopes were controlled using Metamorph 7 software (MDS Analytical Technologies, Sunnyvale, CA, USA).

For calculating the CCS nucleation index, each new appearance of μ2-adaptin-mCherry–marked CCSs was manually counted on segmented fibers, and results were expressed as a function of fiber length and time. For calculating the CCS lifetime, persistence of μ2-adaptin-mCherry–marked CCSs was manually tracked over time. At least 700 CCSs from at least 15 cells per condition and per experiment were analyzed in three to five independent experiments.

CCS and actin retrograde flow measurements

To image CCS retrograde flow, MDA-MB-231 cells were transfected with a GFP-tagged α-adaptin subunit of AP-2 24 hours after cell plating using Lipofectamine 3000 (Thermo Fisher Scientific) according to the manufacturer's instructions. Cells treated or not with 50 μM blebbistatin were imaged for 30 min to 1 hour with an image every 10 s using a spinning disk microscope based on a CSU22 Yokogawa head mounted on the lateral port of an inverted TE-2000U Nikon microscope equipped with a 100× 1.4 NA Plan-Apo and a laser combiner system, which included 491- and 561-nm 50-mW lasers. The microscopes were controlled using Metamorph 7 software (MDS Analytical Technologies, Sunnyvale, CA, USA). CCSs were manually tracked using Metamorph, and at least 45 CCSs were tracked per condition in three to five cells. To visualize both actin retrograde flow and CCSs, MDA-MB-231 cells were transfected with both the GFP-tagged heavy chain of myosin-II and mCherry-tagged μ2-adaptin subunit of AP-2 using the transfection protocol and microscope setup described above. Manual CCS tracking was performed using Metamorph.

Collagen fiber remodeling assay

To investigate the role of actin in collagen remodeling, 150,000 MDA-MB-231 cells (treated or not with blebbistatin) were spotted at 37°C on a coverslip coated with Alexa548-conjugated collagen

fibers. After 1.5 hours of incubation, cells were fixed in PFA and processed for immunofluorescence microscopy by using A488-labeled phalloidin. Z-stacks were generated from images taken at 0.1-μm intervals. Images were analyzed using ImageJ, and the height of collagen fibers in relation with the total height of the cell was calculated. For illustration purposes, phalloidin z-stacks were transformed into z-projection, while collagen fiber z-stacks were transformed into a single image with a color code for different height. At least 20 cells per condition and per experiment were analyzed in two independent experiments.

To investigate the differential remodeling of naked versus EGF- or LDL-decorated fibers, the two kinds of fibers were sequentially spotted on glass-bottom 96-well plates before 65,000 control, or siRNA-treated, or gefitinib-treated MDA-MB-231 cells were seeded per well in DMEM supplemented with 1% FCS and penicillin-streptomycin. Plates were then immediately imaged at 37°C and 5% CO_2 by spinning disk microscopy. One frame was collected every 20 min for 6 hours. Naked and decorated fibers were individually segmented, and remodeling over time was quantified as a function of the evolution of collagen fiber circularity index using the following ImageJ macro:

```
for (i = 0; i < 10; i++) {
run("Subtract Background...", "rolling=10 stack");
setAutoThreshold("Default dark");
//run("Threshold...");
setOption("BlackBackground", false);
setThreshold(XX,100000);
run("Convert to Mask", "method=Default background=Dark");
run("Remove Outliers...", "radius=0.5 threshold=50 which=Dark stack");
run("Analyze Particles...", "size=10-Infinity show=Nothing summarize stack");
close();
}
```

The threshold (XX) was manually defined for each fiber type and for each experiment. At least six wells per condition and per experiment were analyzed in three to four independent experiments.

Traction force microscopy

Glass-bottom FluoroDishes were treated with 3-aminopropyltrimethoxysilane (Sigma-Aldrich, St. Louis, MO). Dishes were then washed three times with water before being treated for 30 min with 0.5% glutaraldehyde and then washed again once with water. To produce gels with a Young's modulus of 5 kPa, 40% acrylamide and 2% bis-acrylamide (Bio-Rad Laboratories, Richmond, CA) were mixed in PBS. For traction force measurements, FluoSpheres (0.2 μm, 660 to 680 nm; Invitrogen) were embedded in the gel (5% volume). Polymerization was initiated using ammonium persulfate and *N*,*N*,*N*,*N*-tetramethylethylenediamine. The gel was then poured between the prepared FluoroDish and an 18-mm glass coverslip and allowed to polymerize for 60 min. After removing the glass coverslip in PBS, the gel on the FluoroDish was functionalized through incubation in a buffer containing 50 mM Hepes (pH 7.5), 1-ethyl-3-[3-dimethylaminopropyl] carbodimide hydrochloride (10 mg/ml) (Thermo Fisher Scientific), and Sulfo-SANPAH (1 mg/ml; Pierce) for 30 min at RT. The gel was then exposed to ultraviolet for 10 min and washed with PBS before being coated with protein G (20 μg/ml) for 2 hours at 37°C, washed three times with PBS, and incubated with 4 μg of anti–collagen I antibody at 37°C overnight. The next day, after several washes with PBS, 15 μl of either Alexa488-EGF–decorated or nondecorated Alexa488-labeled collagen fibers was spotted for 10 min three times in a row, before being washed three times with PBS. Complete medium (1 ml) was added to cover the gel. Once the FluoroDishes at the microscope, 30,000 MDA-MB-231 cells per dish were added and allowed to spread for 10 min. Fluorescence images of beads and fibers and a phase-contrast image were recorded every 2 min for 1 hour. At the end of the measurement, cells were detached by adding 10 μM cytochalasin D (Sigma-Aldrich) and 0.5% Triton (Euromedex), and a reference image without cells was acquired. Z-stacks of 30 images with a distance of 1 μm were acquired to select the best focus (Metamorph software). We used a previously described correlation algorithm to extract the bead displacement fields (*26*) and extract the strain energy that corresponds to the energy the cell exerted to deform the gel and that is proportional to the average tension applied by the cell.

3D migration assays

To evaluate EGF stability on collagen fibers, EGF-decorated 3D collagen networks were imaged 1 hour after polymerization or after 24 hours of incubation at 37°C. Uniform networks were imaged randomly, while composite networks were imaged at the interface between naked and EGF-decorated networks.

For the spreading analysis in 3D, control or siRNA-treated MDA-MB-231 cells were embedded in uniform 3D networks composed of either naked or EGF-coated collagen fibers in 96-well plates and imaged with a wide-field microscope 24 hours later. Cell circularity was measured using ImageJ. At least 70 cells per condition and per experiment were quantified in three independent experiments. Data are expressed as average, inversed circularity.

For migration assays in 3D collagen networks, control or siRNA-treated MDA-MB-231 cells in the presence of DMEM supplemented with 10% FCS were imaged between 1 and 36 hours after being embedded in the gel by spinning disk microscopy through a 10× objective. To measure cell velocity in uniform networks, frames were collected every 20 min for 10 hours, and cells were manually tracked using ImageJ. For composite networks, we chose areas of the gel where both nondecorated and decorated regions were visible. Frames were collected every 20 min for 10 hours. Cells were manually tracked using ImageJ and separated into three categories: cells only evolving in the nondecorated network, cells only evolving in the decorated network, and cells reaching at some point the interface between decorated and nondecorated networks. In that latter case, an initial tracking point was set when cells reached the interface, if they were not already at the interface at the beginning of the movie. Data are represented via track plots produced by the ImageJ plugin chemotaxis tool (Ibidi). At least 18 cells per condition and per experiment were tracked in at least three independent experiments. For condition with cells treated with siRNAs or for control experiment with composite gels composed of two nondecorated networks, only cells leaving the interface were analyzed. Cells were ranked on the basis of whether they leave the interface to go toward the nondecorated or EGF/LDL-decorated networks. At least 63 cells per condition were quantified in at least three to six independent experiments.

Statistical analyses

Statistical analyses in Figs. 1 (E and G), 2 (B, G, and I), 3 (B and G to J), and 4 (B, E, and F) and figs. S3C, S4H, S6 (C to E), and S7E have been performed using Kruskal-Wallis one-way analysis of variance (ANOVA) followed by an all pairwise multiple comparison procedure (Tukey test). Data in Figs. 2 (E, F, and J) and 3 (D and F) and figs. S3 (A, D, E,

and H), S4 (A, C, E, G, and J), S5B, S6F, and S7 (A, B, and D) have been tested using Student's *t* test. All statistical analyses were performed using SigmaStat software.

SUPPLEMENTARY MATERIALS

Supplementary material for this article is available at https://science.org/doi/10.1126/sciadv.abf4647

View/request a protocol for this paper from *Bio-protocol*.

REFERENCES AND NOTES

1. H. T. McMahon, E. Boucrot, Molecular mechanism and physiological functions of clathrin-mediated endocytosis. *Nat. Rev. Mol. Cell Biol.* **12**, 517–533 (2011).
2. G. Montagnac, A. Echard, P. Chavrier, Endocytic traffic in animal cell cytokinesis. *Curr. Opin. Cell Biol.* **20**, 454–461 (2008).
3. T. Maritzen, H. Schachtner, D. F. Legler, On the move: Endocytic trafficking in cell migration. *Cell. Mol. Life Sci.* **72**, 2119–2134 (2015).
4. N. Elkhatib, E. Bresteau, F. Baschieri, A. L. Rioja, G. Van Niel, S. Vassilopoulos, G. Montagnac, Tubular clathrin/AP-2 lattices pinch collagen fibers to support 3D cell migration. *Science* **356**, eaal4713 (2017).
5. F. Baschieri, K. Porshneva, G. Montagnac, Frustrated clathrin-mediated endocytosis-causes and possible functions. *J. Cell Sci.* **133**, jcs240861 (2020).
6. R. O. Hynes, A. Naba, Overview of the matrisome-An inventory of extracellular matrix constituents and functions. *Cold Spring Harb. Perspect. Biol.* **4**, a004903 (2012).
7. R. O. Hynes, The extracellular matrix: Not just pretty fibrils. *Science* **326**, 1216–1219 (2009).
8. Y. Yang, Y. Zhao, B. Chen, Q. Han, W. Sun, Z. Xiao, J. Dai, Collagen-binding human epidermal growth factor promotes cellularization of collagen scaffolds. *Tissue Eng. Part A* **15**, 3589–3596 (2009).
9. J. Wyckoff, W. Wang, E. Y. Lin, Y. Wang, F. Pixley, E. R. Stanley, T. Graf, J. W. Pollard, J. Segall, J. Condeelis, A paracrine loop between tumor cells and macrophages is required for tumor cell migration in mammary tumors. *Cancer Res.* **64**, 7022–7029 (2004).
10. S. J. Wang, W. Saadi, F. Lin, C. Minh-Canh Nguyen, N. Li Jeon, Differential effects of EGF gradient profiles on MDA-MB-231 breast cancer cell chemotaxis. *Exp. Cell Res.* **300**, 180–189 (2004).
11. P. Nievelstein-Post, G. Mottino, A. Fogelman, J. Frank, An ultrastructural study of lipoprotein accumulation in cardiac valves of the rabbit. *Arterioscler. Thromb.* **14**, 1151–1161 (1994).
12. M. H. Cohen, G. A. Williams, R. Sridhara, G. Chen, W. D. McGuinn, D. Morse, S. Abraham, A. Rahman, C. Liang, R. Lostritto, A. Baird, R. Pazdur, United States Food and Drug Administration drug approval summary: Gefitinib (ZD1839; Iressa) tablets. *Clin. Cancer Res.* **10**, 1212–1218 (2004).
13. A. P. Liu, F. Aguet, G. Danuser, S. L. Schmid, Local clustering of transferrin receptors promotes clathrin-coated pit initiation. *J. Cell Biol.* **191**, 1381–1393 (2010).
14. A. Wilde, E. C. Beattie, L. Lem, D. A. Riethof, S. H. Liu, W. C. Mobley, P. Soriano, F. M. Brodsky, EGF receptor signaling stimulates SRC kinase phosphorylation of clathrin, influencing clathrin redistribution and EGF uptake. *Cell* **96**, 677–687 (1999).
15. L. E. Johannessen, N. M. Pedersen, K. W. Pedersen, I. H. Madshus, E. Stang, Activation of the epidermal growth factor (EGF) receptor induces formation of EGF receptor- and Grb2-containing clathrin-coated pits. *Mol. Cell. Biol.* **26**, 389–401 (2006).
16. M. Ehrlich, W. Boll, A. Van Oijen, R. Hariharan, K. Chandran, M. L. Nibert, T. Kirchhausen, Endocytosis by random initiation and stabilization of clathrin-coated pits. *Cell* **118**, 591–605 (2004).
17. D. Loerke, M. Mettlen, D. Yarar, K. Jaqaman, H. Jaqaman, G. Danuser, S. L. Schmid, Cargo and dynamin regulate clathrin-coated pit maturation. *PLOS Biol.* **7**, 0628–0639 (2009).
18. C. Lamaze, S. L. Schmid, Recruitment of epidermal growth factor receptors into coated pits requires their activated tyrosine kinase. *J. Cell Biol.* **129**, 47–54 (1995).
19. T. Sorkina, F. Huang, L. Beguinot, A. Sorkin, Effect of tyrosine kinase inhibitors on clathrin-coated pit recruitment and internalization of epidermal growth factor receptor. *J. Biol. Chem.* **277**, 27433–27441 (2002).
20. Q. Wang, G. Villeneuve, Z. Wang, Control of epidermal growth factor receptor endocytosis by receptor dimerization, rather than receptor kinase activation. *EMBO Rep.* **6**, 942–948 (2005).
21. Q. Wang, X. Chen, Z. Wang, Dimerization drives EGFR endocytosis through two sets of compatible endocytic codes. *J. Cell Sci.* **128**, 935–950 (2015).
22. P. May, J. Herz, H. H. Bock, Molecular mechanisms of lipoprotein receptor signalling. *Cell. Mol. Life Sci.* **62**, 2325–2338 (2005).
23. T. Tojima, R. Itofusa, H. Kamiguchi, Asymmetric clathrin-mediated endocytosis drives repulsive growth cone guidance. *Neuron* **66**, 370–377 (2010).
24. C. Kural, A. A. Akatay, R. Gaudin, B. C. Chen, W. R. Legant, E. Betzig, T. Kirchhausen, Asymmetric formation of coated pits on dorsal and ventral surfaces at the leading edges of motile cells and on protrusions of immobile cells. *Mol. Biol. Cell* **26**, 2044–2053 (2015).
25. F. Baschieri, D. Le Devedec, S. Tettarasar, N. Elkhatib, G. Montagnac, Frustration of endocytosis potentiates compression-induced receptor signaling. *J. Cell Sci.* **133**, jcs239681 (2021).
26. N. Elkhatib, M. B. Neu, C. Zensen, K. M. Schmoller, D. Louvard, A. R. Bausch, T. Betz, D. M. Vignjevic, Fascin plays a role in stress fiber organization and focal adhesion disassembly. *Curr Biol.* **24**, 1492–1499 (2014).

Acknowledgments: We wish to thank the imaging facilities of Gustave Roussy and Institut Curie for help with image acquisition. **Funding:** Core funding for this work was provided by the Gustave Roussy Institute and the Inserm, and additional support was provided by grants from ATIP/Avenir Program, la Fondation ARC pour la Recherche sur le cancer, Le Groupement des Entreprises Françaises dans la LUtte contre le Cancer (GEFLUC), Institut Nationale du Cancer (INCA 2018-1-PL BIO-02-IGR-1), and the Fondation pour la Recherche Médicale (FRM DEQ20180339205) to G.M. This project was supported by grant "Taxe d'apprentissage Gustave Roussy-2016-EB." **Author contributions:** E.B. designed and performed the experiments, analyzed the results, and wrote the manuscript. F.B., N.E., K.B., and M.G. performed the experiments. G.M. supervised the study, designed the experiments, and wrote the manuscript. **Competing interests:** The authors declare that they have no competing interests. **Data and materials availability:** All data needed to evaluate the conclusions in the paper are present in the paper and/or the Supplementary Materials.

Submitted 28 October 2020
Accepted 17 September 2021
Published 5 November 2021
10.1126/sciadv.abf4647

ScienceAdvances

Clathrin-coated structures support 3D directed migration through local force transmission

Enzo BresteauNadia ElkhatibFrancesco BaschieriKaren BellecMélanie GuérinGuillaume Montagnac

Sci. Adv., 7 (45), eabf4647. • DOI: 10.1126/sciadv.abf4647

Science Advances (ISSN) is published by the American Association for the Advancement of Science. 1200 New York Avenue NW, Washington, DC 20005. The title *Science Advances* is a registered trademark of AAAS.